Nano-targeting of Mucosal Addressin Cell Adhesion Molecule-1 Identifies Bowel Inflammation Foci in Murine Model

Marta Truffi[1], Miriam Colombo[2]*, Jesus Peñaranda Avila[2], Luca Sorrentino[1], Francesco Colombo[3], Matteo Monieri[1], Veronica Collico[2], Pietro Zerbi[1,4], Erika Longhi[1], Raffaele Allevi[1], Davide Prosperi[2]**, Fabio Corsi[1,5]***

[1] Department of Biomedical and Clinical Sciences "L. Sacco", University of Milan, via G. B. Grassi 74, 20157 Milan, Italy

[2] NanoBioLab, Department of Biotechnologies and Biosciences, University of Milano-Bicocca, Piazza della Scienza 2, 20126 Milan, Italy

[3] Surgery Department, IBD Unit, ASST Fatebenefratelli Sacco – Luigi Sacco University Hospital, via G. B. Grassi 74, 20157 Milan, Italy

[4] Pathology Department, ASST Fatebenefratelli Sacco-Luigi Sacco Hospital, via G. B. Grassi 74, 20157 Milan, Italy

[5] Surgery Department, Breast Unit, ICS Maugeri S.p.A. SB, via S. Maugeri 10, 27100 Pavia, Italy

** These Authors have equally contributed*

***Corresponding authors:*

Fabio Corsi

University of Milan, Via G. B. Grassi 74, 20157 Milan, Italy; +39 0250319850-19858; fabio.corsi@unimi.it

Davide Prosperi

University of Milano-Bicocca, Piazza della Scienza 2, 20126 Milan, Italy; +39 0264483302; davide.prosperi@unimib.it

Financial disclosure:

This work was supported by Fondazione Regionale per la Ricerca Biomedica (FRRB) and Academic Funding Unimib 2016. “Assessorato alla Sanità”, Regione Lombardia, made a financial contribution in the beginning of the project (funding addressed to “NanoMeDia” project). All the authors declare that there are no conflicts of interest for this work.

Acknowledgements:

M.T. and M.M. are grateful to FRRB for research fellowships. V.C. and J.P.A are grateful for fellowship by Academic Funding Unimib 2014. M.C., D.P. and F.C. thank FRRB for financial support to this study.

Ethical conduct of research

The experimental protocol of the study was subjected to direct approval of the Italian Ministry of Health. Animal care was in accordance with institution guidelines.

Abstract

Aims: We investigate mucosal addressin cell-adhesion molecule (MAdCAM)-1 as a reliable target to detect active bowel inflammation for selective non-invasive nanodiagnostics.

Materials and Methods: We coupled anti-MAdCAM-1 antibodies to manganese oxide nanoparticles, and analyzed nanoconjugate biodistribution and safety in murine model of inflammatory bowel disease by imaging and histology.

Results: Nanoparticles were stable and non-toxic. Upon administration in colitic mice, anti-MAdCAM-1-functionalized nanoparticles preferentially localized in the inflamed bowel, whereas untargeted nanoparticles were more rapidly washed out. Nanoparticles did not induce lesions in non-target organs.

Conclusions: Anti-MAdCAM-1-functionalized nanoparticles detected active bowel inflammation foci, accurately following MAdCAM-1 expression pattern. These nanoconjugates could be a promising non-invasive imaging system for an early and accurate follow-up in patients affected by acute colitis.

Keywords: manganese oxide nanoparticles, MAdCAM-1, inflammatory bowel diseases, imaging

Introduction

In recent years, a global rising of incidence of inflammatory bowel diseases (IBD) has been observed.[1-3] The European Crohn's and Colitis Organization (ECCO) stated that clinical stadiation and follow-up of IBD includes ileo-colonoscopy with biopsies to assess the presence and the severity of the disease.[4] Endoscopy allows clinicians to exclude recurrence and to verify mucosal healing after therapy; moreover, accuracy of ileo-colonoscopy is significantly higher than imaging for terminal ileum diagnostics, especially for mild lesions.[5] Therefore, millions of people worldwide annually undergo invasive procedures for proper follow-up of their disease, with a negative impact on quality of life and a major psychological burden.[6,7] In the emergency setting, acute severe colitis requiring urgent colectomy could be avoided in some cases by an early recognition of increased severity of IBD, leading to a proper therapy escalation [8]. In other cases, the early recognition of therapy failure could lead to prompt urgent colectomy, thus avoiding higher complications rate and mortality, which are often described with delayed surgery for misdiagnosed refractory colitis [9]. This fact is particularly relevant in paediatric ulcerative colitis, since an accurate and early assessment or therapy response predicts the clinical course of the disease and the need of medical salvage therapy [10]. Evaluation of acute colitis in IBD could be completed by computed tomography (CT) scan or ultrasound [4]. However these techniques rely on aspecific radiological signs of bowel inflammation, such as contrast enhancement of bowel wall thickening, and specific targeted imaging is still lacking.[11] Consequently the current best clinical management for IBD evaluation only offers an approximation of the real clinical scenario, and an accurate stadiation of IBD for assessment of response to therapies or indication for surgery is challenging.

Mucosal addressin cell-adhesion molecule-1 (MAdCAM-1) has been proposed as a marker of bowel inflammation. It is upregulated on gut endothelium in IBD at very early stages of the disease, and is responsible for recruiting T cells by binding the integrin $\alpha_4\beta_7$, with subsequent promotion of chronic inflammation in involved bowel tracts.[12,13] Interestingly, MAdCAM-1 is also finely related to IBD onset and activity, and plays a role in the response to therapy, since its expression is higher in non-responder patients and decreases in case of remission after anti-TNFα treatment.[14] In recent years, it is emerging that targeting leukocyte homing is a successful strategy for induction and maintenance of remission in IBD, and open new concept in IBD management.[15-18]

Here, MAdCAM-1 was investigated as a reliable and early IBD-related endothelial target to be exploited for site-specific nanotheranostics in a murine model of acute bowel inflammation. Indeed, oral administration of dextran sodium sulfate (DSS) for a short period of time is widely used in preclinical research to induce reproducible colitis in mice.[19] This model reproduces some morphological features of human colitis, including leukocytes infiltration, increased production of proinflammatory factors, and over-expression of adhesion molecules. Moreover, it has been demonstrated that ablation or inhibition of MAdCAM-1 ameliorates colitis in DSS-induced IBD.[20,21] From these concerns, we reasoned that DSS-induced acute bowel inflammation could have been suitable to investigate MAdCAM-1 as an early and IBD-related molecular target. Anti-MAdCAM-1 antibody was conjugated to a smart and safe delivery nanoparticle, consisting of a manganese oxide *core* coated with an amphiphilic polymer. This nanoparticle could hold multifunctional properties, deriving from both the magnetic property of the *core* and the surface functionalization, to implement imaging and targeted drug delivery. Nanomedicine offers exclusive opportunities to design novel imaging agents and targeted therapeutic carriers, thanks to tunable properties of nanomaterials, which make them particularly appreciable for several biomedical applications.[22] In particular, nuclear spin-active metal nanocrystals, including iron(II,III), Mn(II) and Gd(III) oxides, exhibit unique paramagnetic properties that make them suitable as powerful contrast enhancers in MRI. While superparamagnetic iron oxide nanoparticles (Fe_3O_4 and γ-Fe_2O_3) are extensively utilized as contrast agents in T_2-weighted images,[23,24] MnO and Gd_2O_3 nanoparticles can be exploited for positive contrast in T_1-weighted imaging, leading to bright signal in correspondence to nanoparticle accumulation in specific tissue areas.[25,26] This effect could be of great utility for imaging of the bowel, which provides intrinsically dark MRI in absence of contrast enhancers.

The aim of this study was to assess the targeting efficacy and the accuracy of innovative low-toxic MnO nanoparticles functionalized with anti-MAdCAM-1 antibodies, specifically designed to detect active bowel inflammation foci at early stages of the disease. Pursuing this targeted strategy has the potential to provide a non-invasive and specific system to improve clinical care and management of IBD patients.

Materials and Methods

Synthesis of MnO nanoparticles

The synthesis of MnO nanoparticles (MnO NPs) was carried out according to a two-steps protocol previously described,[25] consisting of the synthesis of the precursor from a metal salt and its subsequent solvothermal decomposition (see Supplementary Information for details). Phase transfer from chloroform to water solution was achieved by coating the nanoparticles with a modified poly(isobutylene-alt-maleic anhydride) (PMA), according to a previously reported procedure.[27,28] Then, the suspension was dried and further redispersed in sodium borate buffer (3 mL) at pH 12 by sonication. Nanoparticles were three times washed and centrifuged (811 ×g, 10 min, Scanspeed 173OR, Labogene), purified by gel electrophoresis as described elsewhere,[29] and finally resuspended in deionized water at a stock concentration (MnO-PMA NPs).

Nanoparticles characterization

Nanoparticle hydrodynamic size was determined by dynamic light scattering (DLS) using a Malvern® 90 Plus DLS instrument (15 mW solid state laser). Backscattered light at a fixed scattering angle of 173° was collected to provide the scattering signal. MnO and MnO-PMA NPs samples were prepared by diluting the stock solution in a disposable cuvette with 1 cm optical length in ultrapure water to 50 μg mL^{-1} and allowed to equilibrate at 25 °C for 30 s before analysis. Mean hydrodynamic diameter and standard deviation were calculated with multimodal analysis by Mie theory, considering absolute viscosity and refractive index values of the medium to be 0.911 cP and 1.330 for water and 0.542 cP and 1.446 for chloroform, respectively. Three replicate measurements per sample were performed to establish the measurements reliability. ζ-potential was determined with the same instrument equipped with DTS1070 electrode and data were processed by ZetaPlus Software. ζ-potential was calculated from electrophoretic mobility based on Smoluchowski equation. A viscosity of 0.911 cP, a dielectric constant of 78.5, and Henry function of 1.5 were used for the calculations. The results were expressed as mean ± standard deviation (SD) of three measurements. Transmission electron microscopy (TEM) images were obtained with a Zeiss EM-109 microscope operating at 80 kV. The sample (2 μL, 0.1 μg mL^{-1}) was deposited onto a 200-mesh

formvar/carbon-coated copper grid (Ted Pella, Redding, CA, USA), and air-dried before examination. The particle size distribution and the average particle size were calculated measuring at least 200 particles by a Measure IT Olympus Software.

Surface functionalization with antibodies

MnO-PMA NPs were functionalized with the half-chain of a monoclonal anti-MAdCAM-1 antibody (AP-MAB0842, Abcam) (MnO-MdC) or with a nonspecific anti-rabbit IgG molecule (Sigma-Aldrich) (MnO-IgG). To obtain fluorescent molecules for optical visualization, antibodies were first labeled with the organic dye fluorescein isothiocyanate (FITC),[30] and dissolved in EDTA-PBS (1 mg mL^{-1}). Subsequently, antibodies were added to 2-mercaptoethanolamine kit (MEA, Thermo Scientific) and treated according to the manufacturer's protocol to reduce the disulfide bridges between the two heavy chains. Half-chain quantification was performed by UV-vis analysis at 280 nm wavelength. A 2,2-(ethylenedioxy)bis(ethylamine) aqueous solution (EDBE, 0.05 M, 9 µL) was added to MnO-PMA NPs that were further modified with *N*-succinimidyl-3-(2-pyridyldithio)-propionate (SPDP, 690 µL, 10 mg mL^{-1}) in dimethylsulfoxide, following a previously-established procedure.[30] The resulting thiol-reactive MnO-PMA NPs (1 mg) were incubated at room temperature (RT) for 1 h with 100 µg half-chain antibody (50 µl, 2 mg mL^{-1}). It was estimated an average of 4-5 MdC per nanoparticle, calculated by the UV-visible absorption value of pyridine-2-thione (λ = 343 nm, $\varepsilon = 8.08*10^{\wedge+3}$ M^{-1} cm^{-1}) that detached from SPDP molecule during the MdC antibody conjugation. Eventually, a molar excess of polyethylene glycol (PEG-SH, M_w=500 Da, 100 µg, 10 µl, 10 mg mL^{-1}) was linked covalently to the surface of the NPs to saturate the remaining thiol-reactive functional groups. The excess of reagents was removed by dialysis.

In vitro cytotoxicity studies

SVEC4-10 murine endothelial cell line was purchased by ATCC-LGC Standards (Sesto San Giovanni, IT) and cultured in high glucose Dulbecco's modified Eagle medium (Euroclone S.p.A., Milano, IT) supplemented with 10% heat inactivated fetal bovine serum (Euroclone), 2 mM L-glutamine, 100 U mL^{-1} penicillin, 0.1 mg mL^{-1} streptomycin at 37 °C in a humidified atmosphere containing 5% CO_2. At

confluence, the cells were passaged using trypsin-EDTA (Euroclone). For the cell proliferation assay, cells (5×10^3) were seeded onto 96-well tissue culture plates and incubated with different amounts of MnO-PMA NPs dissolved in the culture medium. At 24, 48 and 72 h, cells were washed with phosphate buffer saline (PBS) and tested with CellTiter 96® AQ_{ueous} Non-Radioactive Cell Proliferation Assay (Promega Italia s.r.l., Milano, IT), according to the manufacturer's instructions. Absorbance was read using a testing wavelength of 490 nm and a reference wavelength of 630 nm. For the apoptosis assay, cells were seeded onto 12-well tissue culture plates, incubated with different amounts of MnO-PMA NPs for 4 or 24 h at 37 °C, washed twice with PBS and treated with the Annexin V-PE-Cy5 Apoptosis Detection Kit (BioVision, Milpitas, US-CA) following the manufacturer's protocol. Cells were analyzed on a FACS Calibur flow cytometer (Becton Dickinson). After gating on viable cells, 10,000 events were acquired for each analysis.

Hemolysis assay

Blood samples from healthy volunteers were freshly collected and centrifuged at 690 ×g for 5 min to isolate packed erythrocytes from the plasma. The pellet was washed three times with sterile PBS 1x (pH 7.4) until supernatant was clear, and finally resuspended 1:10 in sterile PBS. Cell suspension (200 µL) was mixed with 800 µL of MnO-MdC or MnO-IgG NPs suspension at different concentrations (0.005, 0.02 and 0.1 mg mL^{-1} in PBS), gently vortexed and incubated at 37 °C for 30 min, 2 h and 24 h. Double-distilled water and PBS 1x were used as the positive and negative control, respectively. After incubation, samples were centrifuged at 690 ×g for 5 min, and the release of hemoglobin was measured on 100 µL of supernatant by a microplate reader ELx800 (Biotek, Milano, IT) using a testing wavelength of 405 nm. The percentage of hemolysis was calculated as follows: $(Abs_{sample} - Abs_{CTRL-})*100/(Abs_{CTRL+} - Abs_{CTRL-})$. Analysis was performed in triplicate.

Experimental model of colitis

Male C57BL/6 mice (8 weeks old) were purchased from Charles River (Calco, IT), group housed (4 mice/cage) under standard laboratory conditions, and allowed to acclimate for 1 week. Colitis was induced by addition of dextran sulfate sodium salt (DSS, 3% w/v, 40 kDa, MP Biomedicals, Santa Ana, US-CA) to the drinking water, by changing beverage each 2 days. Colitis was monitored daily, by scoring standard

parameters of body weight change, stool consistency and fecal blood, which were summed together to calculate the disease activity index (DAI), as previously described (see Supplementary Information for details).[31,32] After 3, 5 and 7 days of treatment, colon length was measured *ex vivo* with a ruler from the ileum/colon boundary down to the rectum. Dissected bowels were washed with PBS by gentle flushing, and either fixed in 10% formalin for histologic assessment or subdivided into proximal and distal part of colon, snap frozen and used for protein extraction.

Protein extraction and western blotting

Frozen tissues were weighted, homogenized with potter (Glas-Col homogenizer) in 20% w/v Triton lysis buffer (20 mM Tris-HCl pH 7.6, 150 mM NaCl, 1 mM EDTA, 10% Glycerol and 1% Triton X-100), containing 4% Protease Inhibitor Cocktail (Sigma-Aldrich S.r.l., Milan, IT), and cleared at 17,100 ×g for 20 min at 4 °C. A 40 μg aliquot of protein was resuspended in Laemmli buffer, resolved on polyacrylamide gels under reducing conditions and transferred to polyvinylidene difluoride membranes (Immobilon-P, EMD Millipore Corporation, Billerica, MA-US). Membranes were blocked with 5% bovine serum albumin (BSA, Sigma-Aldrich) in Tris buffer saline with 0.1 % Tween-20 (Sigma-Aldrich) for 1 h at RT, and incubated with rat anti-MAdCAM-1 antibody (MECA-367, LifeSpan BioSciences, Seattle, WA) or with rabbit anti-GAPDH (Sigma-Aldrich). Antibodies conjugated to horseradish peroxidase (Abcam) were used as secondary antibodies, and the reaction was developed with the ECL star kit (Euroclone). Densitometric analysis of protein bands was performed with ImageJ software.

Nanoparticles administration and biodistribution analysis

Nanoparticles were administered to mice (n=36) previously treated with DSS for 5 days. The injection was performed in the tail vein upon anesthesia by intraperitoneal injection of avertin (250 μg g^{-1} body weight). Colitic mice were randomly treated with fluorescent-labeled MnO-MdC (n=16) or MnO-IgG (n=16) (5 μg MnO/g body weight). Control colitic mice (n=4) were injected with 0.1 mL sterile saline solution, and used as reference for tissue autofluorescence. At 4 and 24 h post-injection, 8 mice per group were euthanized for analysis of nanoparticle biodistribution and systemic toxicity. Bowel, heart, spleen, lungs, kidneys, liver

were dissected from mice, washed with PBS, wiped, and either analyzed in a IVIS Lumina II imaging system (Calipers Life Sciences, UK) (n=5) or fixed in 10% formalin for histologic assessment (n=3). IVIS images were acquired with a green fluorescent protein emission filter, while excitation was scanned from 430 to 500 nm, and fluorescence was corrected by spectral unmixing for each sample. Epifluorescence intensity was measured in the entire colon of nanoparticles-treated mice, and average autofluorescence measured in the colon of saline-injected mice was subtracted. For normalization of bowel epifluorescence, blood was collected from the retro-orbital plexus of anesthetized mice before euthanasia, and collected in EDTA-coated tubes (Becton Dickinson). Plasma was prepared by centrifugation at 1500 ×g for 15 min at 4 °C and analyzed by spectrofluorimetric analysis (Horiba; λ_{ex} = 480 nm; λ_{em} = 520 nm). Background plasma fluorescence, determined in samples from saline-injected mice, was subtracted from each sample. Normalized colon epifluorescence was then calculated as the ratio between average epifluorescence of the colon and fluorescence intensity measured in the plasma of the same animal.

Histologic assessment

Bowel, liver, kidneys, spleen, heart and lung samples were fixed with 10% buffered formalin for at least 48 h at RT and embedded in paraffin. Three μm sections were cut, stained with haematoxylin and eosin (HE) and examined blindly.

Immunohistochemistry

Three μm paraffin sections were cut, dewaxed in xylene and rehydrated in alcohol. Antigen unmasking was performed in microwave oven (citrate buffer pH 6) for 10 min. Endogenous peroxidase and unspecific binding sites were blocked by using appropriate reagents. Sections were incubated with affinity-purified anti-MAdCAM1 antibody for 2 h at RT in a humid chamber. The reaction was revealed by nonbiotin peroxidase detection system with 3,3'-diaminobenzidine free base (DAB) as chromogen (haematoxylin counterstaining). The omission of primary antibody was used as negative control.

Transmission electron microscopy

Small pieces of proximal and distal colon (n=2) were fixed in 2.5% glutaraldehyde (Electron Microscopy Sciences) in 0.1 M phosphate buffer, pH 7.2, for 2 h. Specimens were rinsed with phosphate buffer, and post-fixed in 1.5% osmium tetroxide (Electron Microscopy Sciences) for 2 h, dehydrated by 70, 90 and 100% EtOH, and embedded in epoxy resin (PolyBed 812 Polysciences Inc). Ultrathin sections were examined by TEM (Zeiss EM109).

Statistical analysis

Statistical analyses were conducted using two-tailed Student's *t*-test. All plots show mean ± standard error (SE). The statistical significance threshold was set at $P < 0.05$.

Study approval

Animal care was in accordance with institution guidelines. The experimental protocol of the study was subjected to the direct approval of the Italian Ministry of Health.

Results

Preparation and characterization of nanoparticles

MnO and MnO-PMA NPs were prepared and stored as stock solutions in chloroform and water, respectively. Hydrodynamic diameter (d), polydispersity index (PdI), and ζ-potential values of NPs are shown in Table 1. MnO and MnO-PMA NPs showed a hydrodynamic diameter of 15.0 nm ± 0.3 nm and 41.1 nm ± 1.9 nm, respectively. MnO-PMA NPs were negatively charged (-44.7 mV ± 0.6 mV). Micrographs of MnO NPs are shown in Figure 1. Size distribution analyses calculated from 200 particles confirmed that NPs were monodispersed.

In vitro biocompatibility of nanoparticles

Cell toxicity effect was investigated by incubating 5, 20 or 100 μg mL^{-1} of MnO-PMA NPs on murine endothelial cells, and assessing cell viability at different time (Figure 2A). MnO-PMA NPs were safe, with only a mild reduction in cell viability at the highest tested dose (19.48 % ± 3.15 reduction, unvaried in time). Apoptosis was investigated after 4 and 24 h of incubation, with no significant difference between control and MnO-PMA NPs-treated cells (Figure 2B). Potential harmful effects of nanoparticles were also analyzed by hemolysis assay on blood samples incubated with increasing concentrations of MnO-MdC or MnO-IgG nanoparticles. Negligible effect (less than 2 % hemolysis) was observed even after 24 h incubation with 100 μg mL^{-1} of nanoparticles (Figure 2C). Taken together, these *in vitro* results indicated a good safety profile for MnO-PMA NPs and suitability for intravenous injection.

MAdCAM-1 expression in IBD experimental model

Aim at testing MnO-PMA NPs *in vivo*, we reproduced a murine acute colitis model by treating mice with 3% DSS over 7 days. DSS treatment progressively induced loss of body weight, diarrhea and rectal bleeding, which were scored daily as clinical parameters associated with active colitis (Figure 3A, B, C). The disease activity index (DAI) revealed an acute phase of bowel inflammation starting at 5 days of treatment (Figure 3D). Bowel damage was first assessed by measuring colon length *ex vivo*. Colon was only slightly reduced after 3 days of treatment, while it drastically shortened by 33.7% and 35.9% after 5 and 7 days, respectively

(Figure 3E). Colon damage was confirmed by histological analysis on bowel tissues: inflammation and ulceration were observed at 5 and 7 days with loss of the epithelial lining of mucosa surface and glands (Figure 3F). No inflammation was demonstrated in control and 3-days-treated mice.

MAdCAM-1 expression profile was analyzed by western blotting on bowel tissue homogenates (Figure 4A, B). DSS induced over-expression of MAdCAM-1 in both proximal and distal colon at 5 and 7 days of treatment (Figure 4B). Interestingly, MAdCAM-1 over-expression was initially higher in the proximal part of the colon than in the distal one (P=0.013). Immunohistochemistry on bowel tissue slides confirmed the increase in MAdCAM-1 upon DSS treatment: very few vessels were stained positive in control and 3-days-treated mice, while MAdCAM-1 staining dramatically increased in mucosal vascular endothelium in the areas of damage after 5 and 7 days (Figure 4C). MAdCAM-1 expression pattern correlated with the histologic assessment of inflammatory lesions (Supplementary Figure 1).

Nano-targeting of the inflamed colon

We first confirmed the targeting capability of MnO-MdC nanoconjugates by *in vitro* immunoprecipitation assay with a purified recombinant murine MAdCAM-1 protein. Results showed effective recognition of the target protein by MnO-MdC NPs, while untargeted MnO-IgG or MnO-PMA did not manage to significantly pull-down MAdCAM-1 protein (see Supplementary Figure 2). Then, fluorescently-labeled MnO-MdC NPs or equal amount of untargeted MnO-IgG NPs were injected into the tail vein of mice treated with DSS for 5 days. At 4 and 24 h post-injection, dissected bowels were analyzed. The injection of either MnO-MdC or MnO-IgG NPs did not impact on the length of colon in DSS-treated mice, which appeared shorter than that of healthy mice (Figure 5A). At 4 h post-injection nanoparticles localized in the bowel of colitic mice, and comparable fluorescence intensity was measured in MnO-MdC- and MnO-IgG-treated bowels. At 24 h post-injection MnO-MdC NPs further accumulated in the bowels of mice, as shown by increased fluorescence as compared to MnO-IgG-treated bowels (Figure 5B, D). Bowel-associated epifluorescence was normalized toward fluorescence measured in the blood of the same mice before euthanasia, and results confirmed the specific localization of MnO-MdC NPs *versus* MnO-IgG NPs in the bowel of DSS-treated mice (Figure 5C). These data demonstrated the capability of MAdCAM-1 targeting to promote the selective accumulation of nanoparticles at the inflamed colon. Interestingly, MnO-MdC NPs preferentially localized in the proximal

colon, hence indicating perfect correlation with MAdCAM-1, whose expression was confirmed high in the cecum of all mice (Figure 5E).

TEM analysis on samples of proximal colon showed MnO-MdC NPs on the apical surface of the endothelium of venules at 24 h post-injection. Nanoparticles attached to the endothelium and triggered invagination of the plasma membrane, thus suggesting specific uptake by endothelium in the inflamed colon (Figure 6).

Biodistribution and safety of nanoparticles

Biodistribution of MnO-MdC NPs and MnO-IgG NPs was determined by analyzing fluorescence in dissected non-target organs. Nanoparticles did not show preferential accumulation in heart, spleen, lungs, kidneys or liver. A mild signal was only detected in liver and kidneys, likely suggesting a potential way of clearance (Table 2). Systemic toxicity was assessed by histopathological examination in selected organs isolated 24 h post-injection. No histological lesions were observed, thus demonstrating safety of intravenous administration of the nanoconjugates (Figure 7).

Discussion

Mortality for acute severe colitis reaches up to 70% if urgent colectomy is not performed, and about one third of patients hospitalized for severe colitis require immediate colectomy [8, 33]. This dramatic conclusion could be the result of steroid refractory IBD. In this scenario, early recognition of worsening colitis could impact on decision-making, by a proper treatment escalation or prompt starting of rescue therapy [8]. However, only clinical signs or aspecific imaging features are currently used to define severity of acute colitis [9, 34]. A delayed recognition of therapy failure means a delayed colectomy, which is associated to higher complications in patients with refractory colitis [9]. Indeed, several therapies are currently available as a salvage treatment in patients affected by severe colitis. Therefore, clinicians are more prone to elongate rescue therapy attempts, and patients could be referred for colectomy only at later stages of the disease, when septic shock is ongoing and malnutrition is worsening. Operating such patients is unsafe, and it carries a higher risk of anastomotic leak, fistula, hemorrhage and need for ileostomy [35]. Therefore, a fast and accurate reassessment for early acute colitis should be mandatory to guarantee the best management of these patients, with a wise and timely treatment.

In this scenario, nanomedicine offers novel solutions for theranostic purposes in various clinical settings. A wide literature exists about the translational potential of nanotechnology in cancer or infectious diseases, but the application to IBD management has been poorly investigated.[36] In this study, we developed a targeted nanoplatform for early recognition of acute colitis. Our findings demonstrated that MAdCAM-1-targeted nanoparticles actively accumulated in inflamed bowel sites due to MAdCAM-1 overexpression in endothelium. At 4 h post-injection, both targeted and untargeted nanoparticles reached the colon, probably due to the extensive inflammation infiltrate from the blood to the inflamed tissue in colitic mice. However, at 24 h, a significant proportion of targeted nanoparticles accumulated in proximal colon, whereas untargeted nanoparticles were mostly washed out. Active targeting of the endothelium within the inflamed bowel was demonstrated by TEM images, and allowed us to identify the sites of bowel inflammation.

The rationale in choosing MAdCAM-1 as target for nanoparticles homing resides in multiple advantages. First, MAdCAM-1 offers high and early correlation with the active bowel inflammation, as demonstrated by the concurrence between MAdCAM-1 expression profile and the histological assessment of active inflammation in colonic mucosa of DSS-treated mice. Targeting leukocyte traffic in inflamed bowel is

currently considered a promising strategy for IBD treatment.[18,37] The GEMINI I and GEMINI II-III trials have demonstrated a substantial clinical benefit with a targeted antibody to $\alpha_4\beta_7$ integrins in patients affected by ulcerative colitis and Crohn's disease, even in case of previous anti-TNF treatment.[38-40] In 2015, the TURANDOT and OPERA trials focused on MAdCAM-1 as a natural ligand of $\alpha_4\beta_7$ integrins.[41,42] Clinical remission was higher in ulcerative colitis and in patients not exposed to anti-TNF treatment, while patients with Crohn's disease were unexpectedly less susceptible to this therapy.[39] These milestone trials indicated a partial success for anti-MAdCAM-1 therapy in IBD; however, they provided encouraging proof of concept that targeting leukocyte traffic may represent a tailored therapy for IBD. MAdCAM-1 targeting could be even more appealing when considering its correlation with both intestinal and extra-intestinal IBD.[43] In our study a certain amount of MnO-MdC NPs was detected in liver, kidneys and lungs. Indeed, lungs and liver can be involved in extra-intestinal inflammatory damage in DSS-induced acute colitis.[44,45] However, the presence of nanoparticles in these off-target districts could also be likely attributable to excretion pathways.

Previous studies on anti-MAdCAM nanoparticle-based strategies for IBD are sporadic and mainly involved gas micro-bubbles to improve contrast-enhancement in bowel ultrasound.[46,47] These studies revealed an unexpected role for targeted nanomedicine in IBD; however, their translation into clinical practice could be limited by pitfalls of bowel ultrasound, which requires high expertise and should be restricted only in tertiary centers.

The choice of MnO NPs is related to the low toxicity and to the paramagnetic properties of the *core* that provides a large exploitable nanoplatform. MnO NPs biocompatibility attested that MnO NPs are safe for cell culture even at high concentrations. For these reasons, MnO NPs could be very promising substitutes for the clinically used gadolinium ions as positive contrast enhancer for IBD imaging.[11] Manganese is expected to overcome major limitations encountered with gadolinium, mainly its toxicity, the narrow imaging window due to short blood circulation time and its drop in relaxivity under high magnetic fields.[48] As a consequence, manganese is potentially preferable for molecular and tissue MRI imaging in T_1-weighted, positive-contrast MRI.[48] Recently, Rimola et al. have pointed out the relevance of discriminating bowel wall thickening due to active inflammation from fibrotic stenosis.[49] This issue is even more challenging in patients that have been previously subjected to gastrointestinal surgery, where

discriminating between active IBD, pathological fibrosis and anastomotic scars is arduous.[49] Accurate contrast enhancement of active IBD, by properly homing MnO to MAdCAM-1-overexpressing bowel sites, is expected to circumvent such limitations and avoid nonspecific enhancements. In view of the remarkable contrast power of MnO NPs in T_1-weighted images, our results strongly suggest future *in vivo* MRI studies.

Conclusions

MAdCAM-1-targeted MnO nanoparticles are very promising tools for accurate and early detection and treatment of active IBD, even in early stages of disease, when damage is demonstrated only by histopathology. Clinical potential of such nanoconjugate is undeniable, considering the ability to discriminate active inflammation from fibro-stenosing alterations even in the post-surgical setting. Further studies by MRI are now mandatory, and could allow to get closer to clinical translation, and to explore therapeutic potentials of targeted nanomedicine in IBD.

Summary points

- Evaluation and management of IBD commonly relies on aspecific signs of bowel inflammation and are currently lacking of early and accurate targeted imaging systems.
- Development of smart MnO nanoparticles conjugated with anti-MAdCAM-1 antibodies for selective detection of active bowel inflammation foci.
- MnO nanoparticles were safe and non-toxic *in vitro* and *in vivo*.
- MAdCAM-1-targeted nanoparticles actively accumulated in inflamed bowel sites in murine model of acute colitis, due to MAdCAM-1 overexpression on gut endothelium.
- MAdCAM-1-targeted MnO nanoparticles could be promising tools for accurate detection and treatment of active IBD.

References

1. Vegh Z, Burisch J, Pedersen N, et al. Incidence and initial disease course of inflammatory bowel diseases in 2011 in Europe and Australia: results of the 2011 ECCO-EpiCom inception cohort. *J Crohns Colitis* 8(11), 1506-15 (2014).

2. Ooi CJ, Makharia GK, Hilmi I, et al. Asia Pacific Consensus Statements on Crohn's disease. Part 1: Definition, diagnosis, and epidemiology: (Asia Pacific Crohn's Disease Consensus--Part 1). *J Gastroenterol Hepatol.* 31(1), 45-55 (2016).

3. Burisch J, Pedersen N, Čuković-Čavka S, et al. East-West gradient in the incidence of inflammatory bowel disease in Europe: the ECCO-EpiCom inception cohort. *Gut* 63(4), 588-97 (2014).

4. ** Magro F, Gionchetti P, Eliakim R, et al. Third European Evidence-Based Consensus on Diagnosis and Management of Ulcerative Colitis. Part 1: Definitions, diagnosis, extra-intestinal manifestations, pregnancy, cancer surveillance, surgery, and ileo-anal pouch disorders. *J Crohns Colitis* Feb 2 (2017).[Epub ahead of print]

5. Horsthuis K, Bipat S, Bennink RJ, Stoker J. Inflammatory bowel disease diagnosed with US, MR, scintigraphy, and CT: meta-analysis of prospective studies. *Radiology* 247(1), 64-79 (2008).

6. * Lönnfors S, Vermeire S, Greco M, et al. IBD and health-related quality of life -- discovering the true impact. *J Crohns Colitis* 8(10), 1281-6 (2014).

7. Wright EK, Kamm MA, De Cruz P, et al. Effect of intestinal resection on quality of life in Crohn's disease. *J Crohns Colitis* 9(6), 452-62 (2015).

8. Andrew RE, Messaris E. Update on medical and surgical options for patients with acute severe ulcerative colitis: What is new? *World J Gastrointest Surg.* Sep 27;8(9), 598-605 (2016).

9. Randall J, Singh B, Warren BF, et al. Delayed surgery for acute severe colitis is associated with increased risk of postoperative complications. *Br J Surg* 97, 404-409 (2010).

10. Schechter A, Griffiths C, Gana JC, et al. Early endoscopic, laboratory and clinical predictors of poor disease course in paediatric ulcerative colitis. *Gut* 64(4), 580-8 (2015).

11. Rimola J, Ordás I, Rodriguez S, et al. Magnetic resonance imaging for evaluation of Crohn's disease: validation of parameters of severity and quantitative index of activity. *Inflamm Bowel Dis.* 17(8), 1759-68 (2011). 12. Souza HS, Elia CC, Spencer J, MacDonald TT. Expression of lymphocyte-endothelial receptor-ligand pairs, alpha4beta7/MAdCAM-1 and OX40/OX40 ligand in the colon and

jejunum of patients with inflammatory bowel disease. *Gut* 45(6), 856-63 (1999).

13. Arihiro S, Ohtani H, Suzuki M, et al. Differential expression of mucosal addressin cell adhesion molecule-1 (MAdCAM-1) in ulcerative colitis and Crohn's disease. *Pathol Int.* 52(5-6), 367-74 (2002).

14. ** Biancheri P, Di Sabatino A, Rovedatti L, et al. Effect of tumor necrosis factor-α blockade on mucosal addressin cell-adhesion molecule-1 in Crohn's disease. *Inflamm Bowel Dis.* 19(2), 259-64 (2013).

15. Feagan BG, Rubin DT, Danese S, et al. Efficacy of Vedolizumab Induction and Maintenance Therapy in Patients With Ulcerative Colitis, Regardless of Prior Exposure to TNF Antagonists. *Clin Gastroenterol Hepatol* Sep 14 (2016).

16. Zundler S, Schillinger D, Fischer A, et al. Blockade of αEβ7 integrin suppresses accumulation of CD8+ and Th9 lymphocytes from patients with IBD in the inflamed gut in vivo. *Gut* Aug 19 (2016).

17. Dulai PS, Sandborn WJ. Next-Generation Therapeutics for Inflammatory Bowel Disease. *Curr Gastroenterol Rep.* 18(9), 51 (2016).

18. Neurath MF. New targets for mucosal healing and therapy in inflammatory bowel diseases. *Mucosal Immunol.* 7(1), 6-19 (2014).

19. Kiesler P, Fuss IJ & Strober W. Experimental models of inflammatory bowel diseases. *Cell Mol. Gastroenterol. Hepatol.* 1, 154-170 (2015).

20. Schippers A, Muschaweck M, Clahsen T, et al. β7-Integrin exacerbates experimental DSS-induced colitis in mice by directing inflammatory monocytes into the colon. *Mucosal Immunol.* 9(2), 527-38 (2016).

21. Kato S, Hokari R, Matsuzaki K, et al. Amelioration of murine experimental colitis by inhibition of mucosal addressin cell adhesion molecule-1. *J Pharmacol Exp Ther.* 295(1), 183-9 (2000).

22. ** Gobbo OL, Sjaastad K, Radomski MW, et al. Magnetic Nanoparticles in Cancer Theranostics. *Theranostics* 5(11), 1249-63 (2015).

23. Na HB, Song IC, Hyeon T. Inorganic nanoparticles for MRI contrast agents. *Adv. Mater.* 21, 2133-2148 (2009).

24. Colombo M, Carregal-Romero S, Casula MF, et al. Biological applications of magnetic nanoparticles. *Chem Soc Rev.* 41(11), 4306-34 (2012).

25. * Na HB, Lee JH, An K, et al. Development of a T1 contrast agent for magnetic resonance imaging using MnO nanoparticles. *Angew Chem Int Ed Engl.* 46(28), 5397-401 (2007).

26. Taylor KML, Rieter WJ, Lin W. Manganese-based nanoscale metal-organic frameworks for

magnetic resonance imaging. *J Am Chem Soc.* 130(44), 14358-9 (2008).

27. Soliman MG, Pelaz B, Parak WJ, Del Pino Pablo. Phase transfer and polymer coating methods toward improving the stability of metallic nanoparticles for biological applications. *Chem. Mater.* 27(3), 990-997 (2015).

28. Pellegrino T, Manna L, Kudera S, et al. Hydrophobic nanocrystals coated with an amphiphilic polymer shell : a general route to water soluble nanocrystals. *Nano Lett.* 4(4), 703-707 (2004).

29. Sperling RA, Pellegrino T, Li JK, et al. Electrophoretic separation of nanoparticles with a discrete number of functional groups. *Adv. Funct. Mater.* 16(7), 943-948 (2006).

30. Fiandra L, Mazzucchelli S, De Palma C, et al. Assessing the in vivo targeting efficiency of multifunctional nanoconstructs bearing antibody-derived ligands. *Acs Nano*. 7(7), 6092-102 (2013).

31. Vetrano S, Rescigno M, Cera MR, et al. Unique role of junctional adhesion molecule-a in maintaining mucosal homeostasis in inflammatory bowel disease. *Gastroenterology* 135(1), 173-84 (2008).

32. Mizushima T, Sasaki M, Ando T, et al. Blockage of angiotensin II type 1 receptor regulates TNF-alpha-induced MAdCAM-1 expression via inhibition of NF-kappaB translocation to the nucleus and ameliorates colitis. *Am J Physiol Gastrointest Liver Physiol.* 298(2), G255-266 (2010).

33. Turner D, Walsh CM, Steinhart AH, Griffiths AM. Response to corticosteroids in severe ulcerative colitis: a systematic review of the literature and a meta-regression. *Clin Gastroenterol Hepatol* 5, 103-110 (2007).

34. Lichtiger S, Present DH, Kornbluth A, et al. Cyclosporine in severe ulcerative colitis refractory to steroid therapy. *N Engl J Med* 330, 1841-1845 (1994).

35. Markel TA, Lou DC, Pfefferkorn M, et al. Steroids and poor nutrition are associated with infectious wound complications in children undergoing first stage procedures for ulcerative colitis. *Surgery* 144, 540-545 (2008).

36. Wu Y, Briley K, Tao X. Nanoparticle-based imaging of inflammatory bowel disease. *Wiley Interdiscip Rev Nanomed Nanobiotechnol.* Sep 15 (2015).

37. Rivera-Nieves J. Strategies that target leukocyte traffic in inflammatory bowel diseases: recent developments. *Curr Opin Gastroenterol.* 31(6), 441-8 (2015).

38. Feagan BG, Rutgeerts P, Sands BE, et al. Vedolizumab as induction and maintenance therapy for ulcerative colitis. *N Engl J Med.* 369(8), 699-710 (2013).

39. Sandborn WJ, Feagan BG, Rutgeerts P, et al. Vedolizumab as induction and maintenance therapy for Crohn's disease. *N Engl J Med.* 369(8), 711-21 (2013).

40. Sands BE, Feagan BG, Rutgeerts P, et al. Effects of vedolizumab induction therapy for patients with Crohn's disease in whom tumor necrosis factor antagonist treatment failed. *Gastroenterology* 147(3), 618-627 (2014).

41. Reinisch W, Sandborn W, Danese S, et al. 901a A randomized, multicenter double-blind, placebo-controlled study of the safety and efficacy of anti-MAdCAM Antibody OF-00547659 (PF) in patients with moderate to severe ulcerative colitis: results of the TURANDOT study. *Gastroenterology* 148:S-1193 (2015).

42. Sandborn W, Lee SD, Tarabar D, et al. 825 anti-MAdCAM-1 antibody (PF-00547659) for active refractory Crohn's disease: results of the OPERA study. *Gastroenterology* 148:S-162 (2015).

43. Adams DH, Eksteen B. Aberrant homing of mucosal T cells and extra-intestinal manifestations of inflammatory bowel disease. *Nat Rev Immunol.* 6(3), 244-51 (2006).

44. Park KS. Lung injury as an extra-intestinal manifestation of inflammatory bowel disease. *Korean J Intern Med.* 31(5), 851-2 (2016).

45. Rullo J, Savatteri M, Fox-Robichaud AE. The role of liver CD1-restricted NK T cells in a model of recurrent colitis. *FASEB J.* 20, A1269 (2006).

46. Bachmann C, Klibanov AL, Olson TS, et al. Targeting mucosal addressin cellular adhesion molecule (MAdCAM)-1 to noninvasively image experimental Crohn's disease. *Gastroenterology* 130(1), 8-16 (2006).

47. Tlaxca JL, Rychak JJ, Ernst PB, et al. Ultrasound-based molecular imaging and specific gene delivery to mesenteric vasculature by endothelial adhesion molecule targeted microbubbles in a mouse model of Crohn's disease. *J Control Release* 165(3), 216-25 (2013).

48. Kanakia S, Toussaint J, Hoang DM, et al. Towards An Advanced Graphene-Based Magnetic Resonance Imaging Contrast Agent: Sub-acute Toxicity and Efficacy Studies in Small Animals. *Sci Reports* 2;5, 17182 (2015).

49. ** Rimola J, Planell N, Rodríguez S, et al. Characterization of inflammation and fibrosis in Crohn's disease lesions by magnetic resonance imaging. *Am J Gastroenterol.* 110(3), 432-40 (2015).

Reference Annotation

[4] This reference is of interest because it represents the latest updated guidelines by the European Crohn's and Colitis Organization (ECCO) for classification, diagnosis and medical management of ulcerative colitis for IBD patients.

[6] A survey at European level on the impact of IBD on patients' quality of life was performed. Most patients claimed that IBD negatively affected their life; therefore it is crucial and urgent to develop efficacious and non-invasive systems able to promote a tailored therapy of IBD without providing additional distress to the patients.

[14] This reference discussed the relevance of MAdCAM-1 protein in IBD pathogenesis and its association with anti-TNF therapies, thus supporting the hypothesis of our study that targeting MAdCAM-1 could be of success.

[22] This review provides an extensive overview on the biomedical applications of magnetic nanoparticles, thus indicating how nanotechnology could promote novel concepts in medicine.

[25] This paper demonstrated the potential of MnO NPs as contrast agent in MRI, and represented a reference for the synthesis of MnO-based nanoparticles used in our study.

[49] This reference focused on the importance of discriminating bowel wall thickening due to active inflammation from fibrotic stenosis. In this perspective, our nanoconjugate is expected to implement the MRI diagnosis of the disease.

Table 1. DLS and TEM analyses of MnO and MnO-PMA NPs.

	Effective diameter (TEM analysis, nm)	Hydrodinamic diameter (DLS analysis, nm)	PdI	ζ -potential (mV)
MnO NPs	9.8 ± 1.3	15.0 ± 0.3	0.148 ± 0.041	-
MnO-PMA NPs	9.9 ± 1.3	41.1 ± 1.9	0.237 ± 0.052	–44.7 ± 0.6

Table 2. Averaged epifluorescence intensity of organs dissected at 4 or 24 h post-nanoparticles-injection. Data are expressed as mean radiant efficiency (p/sec/cm^2/sr)/(μW/cm^2).

Organ	MnO-MdC (× 10^8)		MnO-IgG (× 10^8)	
	4 h	24 h	4 h	24 h
Liver	0.124 ± 0.089	0.102 ± 0.054	0.002 ± 0.002	0.878 ± 0.034
Kidneys	0.178 ± 0.098	0.114 ± 0.064	0.027 ± 0.027	0.348 ± 0.103
Spleen	n.d.	n.d.	n.d.	n.d.
Heart	n.d.	n.d.	n.d.	n.d.
Lungs	0.106 ± 0.065	0.092 ± 0.103	0.042 ± 0.042	0.119 ± 0.048

n.d. not-detectable

Figure Legends

Figure 1. TEM micrograph of MnO NPs. Scale bar: 100 nm.

Figure 2. *In vitro* cytotoxicity study of nanoparticles. (A) Cell viability was assessed by MTS assay upon treatment with MnO-PMA NPs. Mean absorbance of untreated cells (CTRL) was set at 100% viability. Reported values are means ± SE (n=6). (B) The percentage of apoptotic cells was determined at 4 and 24 h of incubation with MnO-PMA NPs and compared to untreated cells (CTRL). Results are means ± SE (n=3). (C) Hemolysis was assessed on blood samples upon incubation with increasing concentrations of MnO-MdC (left panel) or MnO-IgG (right panel) NPs for 30 min, 2 h and 24 h. Results are means ± SE (n=3).

Figure 3. Changes over time in body weight (A), stool consistency (B), and fecal blood (C) were scored daily in control (water) and treated (DSS) mice. (D) Colitis severity was assessed by DAI. (E) Colon length of water-drinking and DSS-treated mice was measured *ex vivo*. Results are means ± SE (n=8). (F) HE of colon sections from control or DSS-treated mice (20× magnification).

Figure 4. MAdCAM-1 expression in colitic bowels. (A) Western blotting of MAdCAM-1 in tissue homogenates of proximal (p) and distal (d) colon from control (water) and treated (DSS) mice. (B) Densitometry of MAdCAM-1 bands normalized to GAPDH. Data are means ± SE (n=4). Asterisks indicate significance of DSS-treated *versus* water-drinking mice; §$P< 0.05$ proximal *versus* distal colon. (C) Representative pictures of MAdCAM-1 immunohistochemistry in colon specimens from control (water) and DSS-treated mice (40× magnification).

Figure 5. Bowel imaging upon nanoparticles exposure. (A) Colon length was measured in colitic mice injected with saline (CTRL) or with MnO-MdC or MnO-IgG NPs, and compared to healthy mice (water). Results are means ± SE. (B) Averaged epifluorescence (Epf) intensity of colon dissected 4 or 24 h post-nanoparticles-injection. Results are means ± SE (n=5). **$P<0.05$ MnO-MdC *versus* MnO-IgG; §$P<0.05$ 24 h *versus* 4 h. (C) Epf intensity of bowels was normalized toward the fluorescence intensity (FI) of plasma collected from the same animal at 24 h. Results are means ± SE (n=5). (D) Epf images of representative bowels from mice exposed to saline (CTRL), MnO-MdC or MnO-IgG NPs for 4 or 24 h. Epf is expressed as

radiant efficiency (p/sec/cm^2/sr)/(μW/cm^2). White lines indicate ileum/colon boundary. (E) MAdCAM-1 immunohistochemistry in cecum specimens: arrows point at MAdCAM-1-positive vessels, asterisks indicate tissue lesions (20× magnification).

Figure 6. TEM images of proximal colon specimens from mice exposed to MnO-MdC NPs for 24 h. Arrows point at a nanoparticle adhering to the endothelium of mucosal venules (scale bar: 500 nm). Higher magnification is shown on the right (scale bar: 200 nm).

Figure 7. Histopathological analysis of non-target organs at 24 h post-nanoparticles-injection (40× magnification).

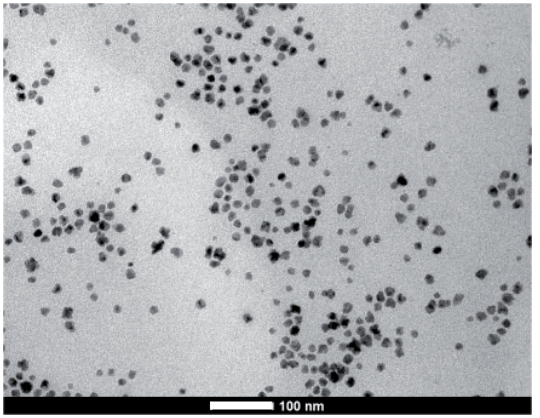
100 nm

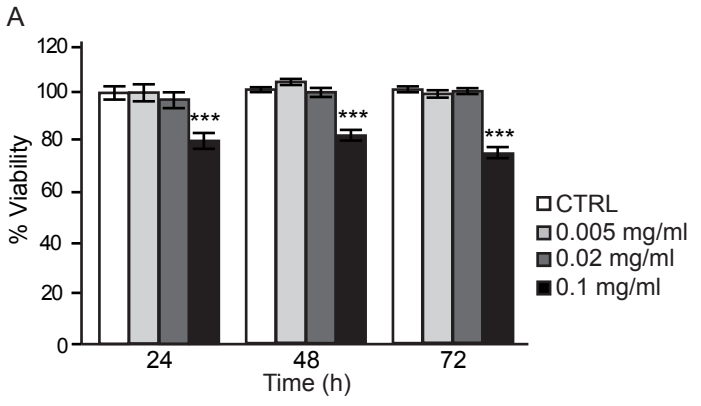
A
120
100
80
60
40
20
0
% Viability
***
***
***
24
48
72
Time (h)
CTRL
0.005 mg/ml
0.02 mg/ml
0.1 mg/ml

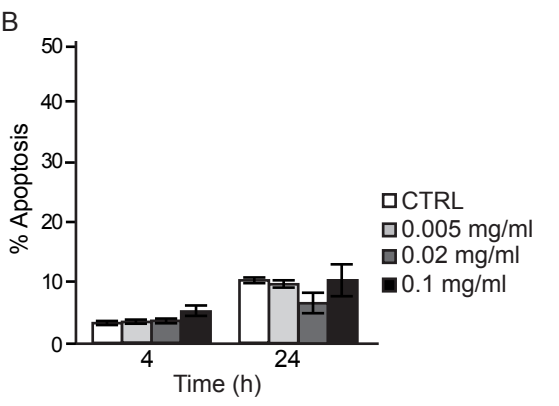
B
50
40
30
20
10
0
% Apoptosis
4
24
Time (h)
CTRL
0.005 mg/ml
0.02 mg/ml
0.1 mg/ml

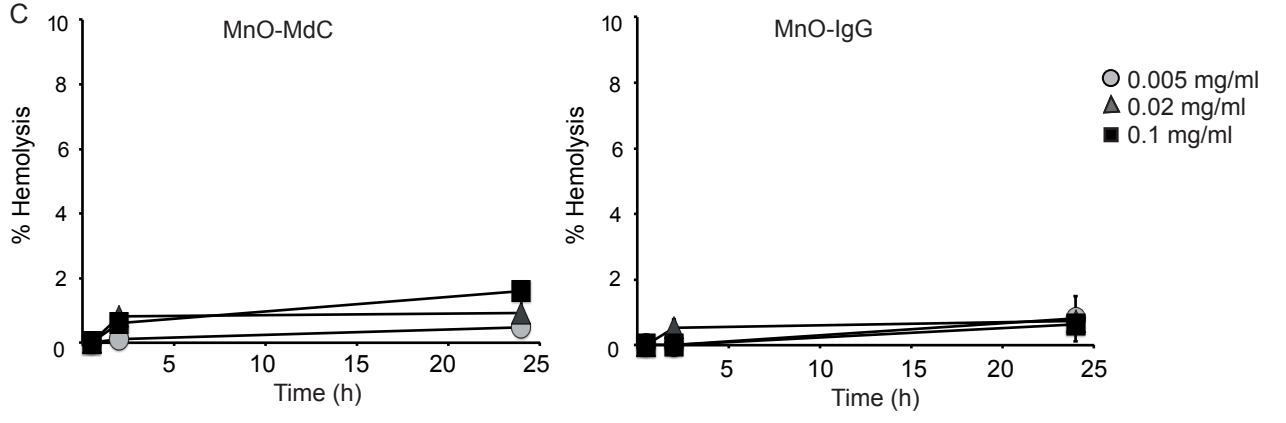
C
MnO-MdC
MnO-IgG
10
8
6
4
2
0
% Hemolysis
5
10
15
20
25
Time (h)
0.005 mg/ml
0.02 mg/ml
0.1 mg/ml

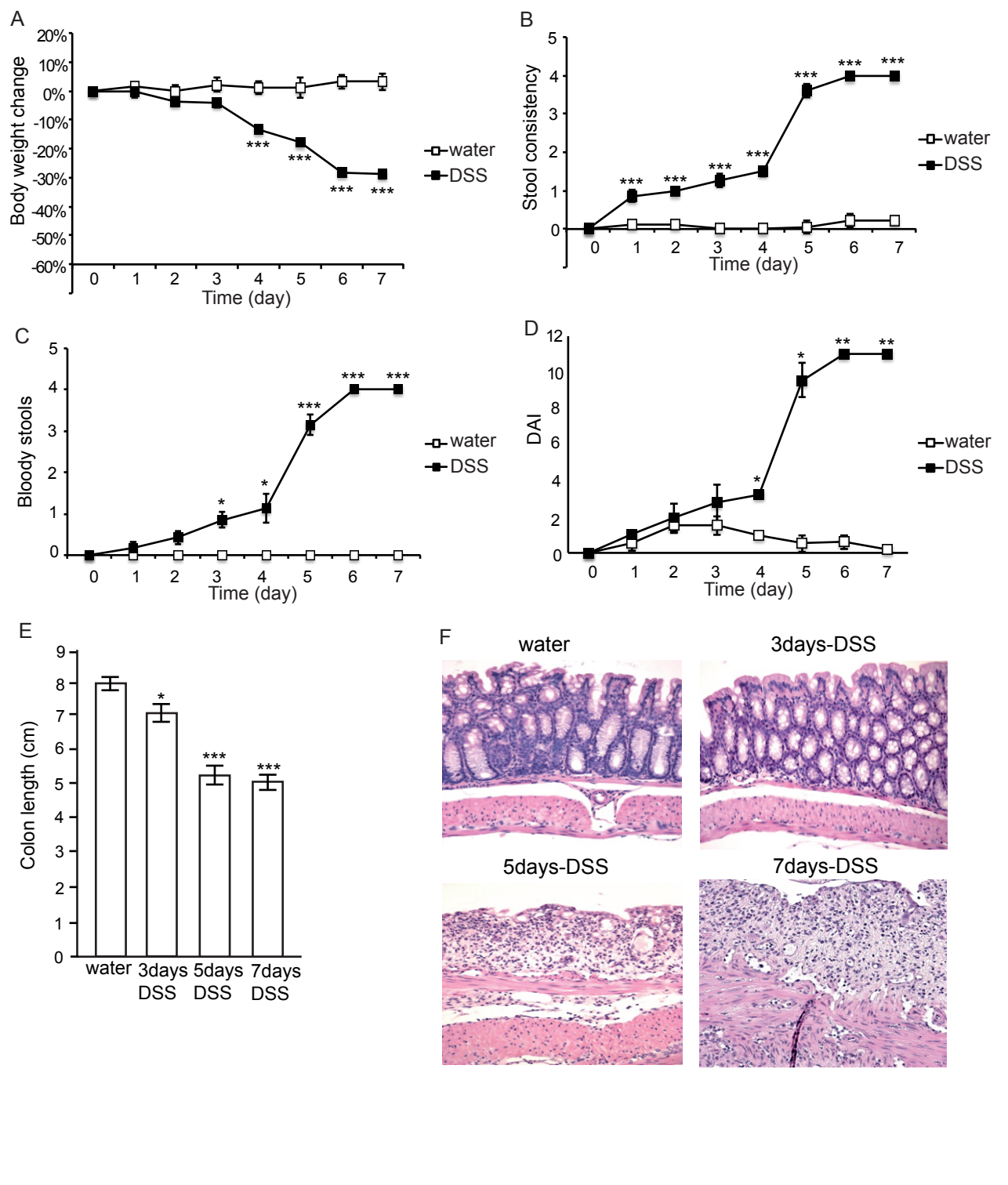
A
Body weight change
20%
10%
0%
-10%
-20%
-30%
-40%
-50%
-60%
0 1 2 3 4 5 6 7
Time (day)
water
DSS
B
Stool consistency
0 1 2 3 4 5
Time (day)
water
DSS
C
Bloody stools
0 1 2 3 4 5
Time (day)
water
DSS
D
DAI
0 2 4 6 8 10 12
Time (day)
water
DSS
E
Colon length (cm)
0 1 2 3 4 5 6 7 8 9
water
3days DSS
5days DSS
7days DSS
F
water
3days-DSS
5days-DSS
7days-DSS

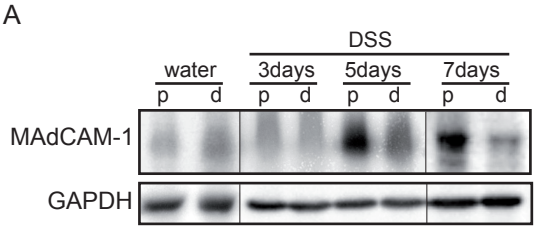
A
DSS
water
3days
5days
7days
p
d
MAdCAM-1
GAPDH

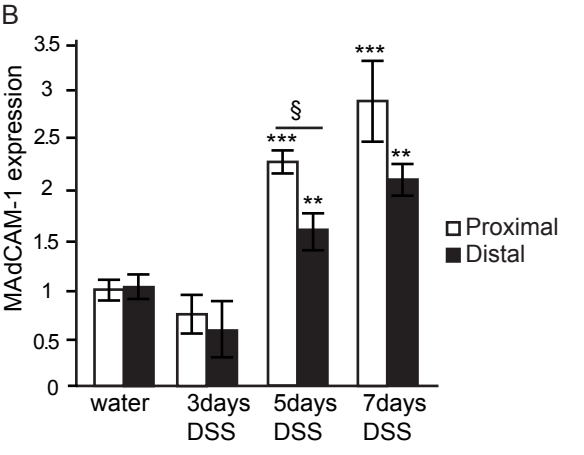
B
MAdCAM-1 expression
3.5
3
2.5
2
1.5
1
0.5
0
§
***
**
water
3days DSS
5days DSS
7days DSS
Proximal
Distal

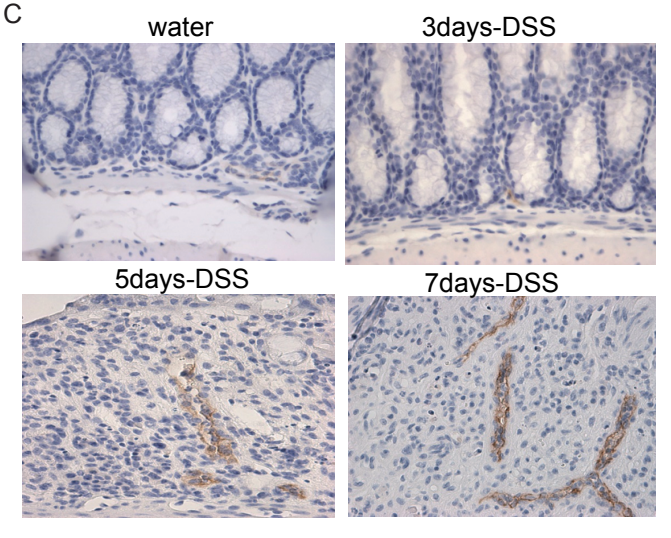
C
water
3days-DSS
5days-DSS
7days-DSS

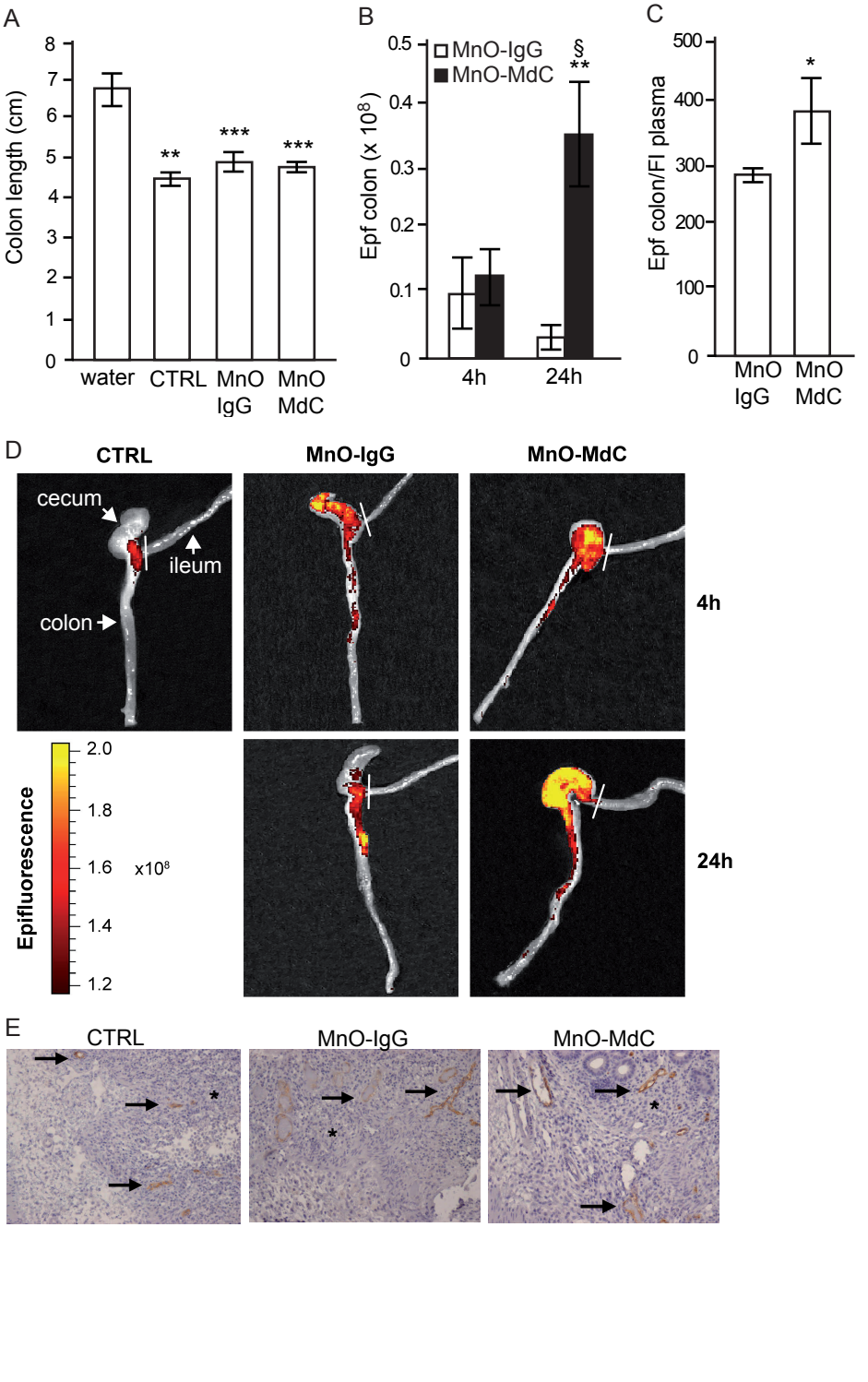
A
Colon length (cm)
water
CTRL
MnO IgG
MnO MdC
B
Epf colon (x 10^8)
MnO-IgG
MnO-MdC
4h
24h
C
Epf colon/Fl plasma
MnO IgG
MnO MdC
D
CTRL
MnO-IgG
MnO-MdC
cecum
ileum
colon
4h
24h
Epifluorescence
x10^8
E
CTRL
MnO-IgG
MnO-MdC

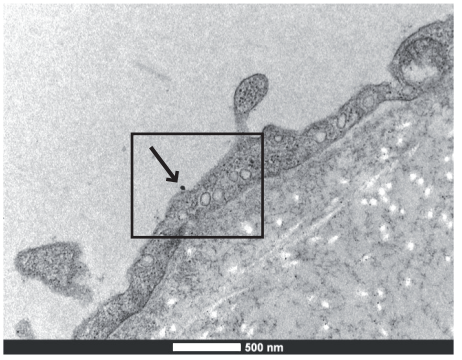
500 nm

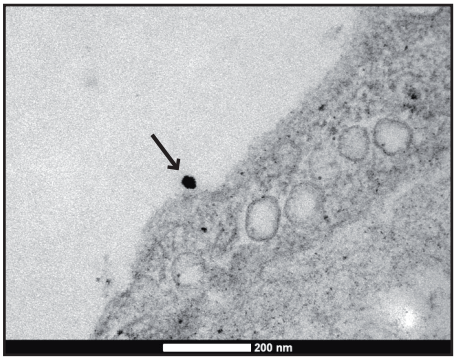
200 nm

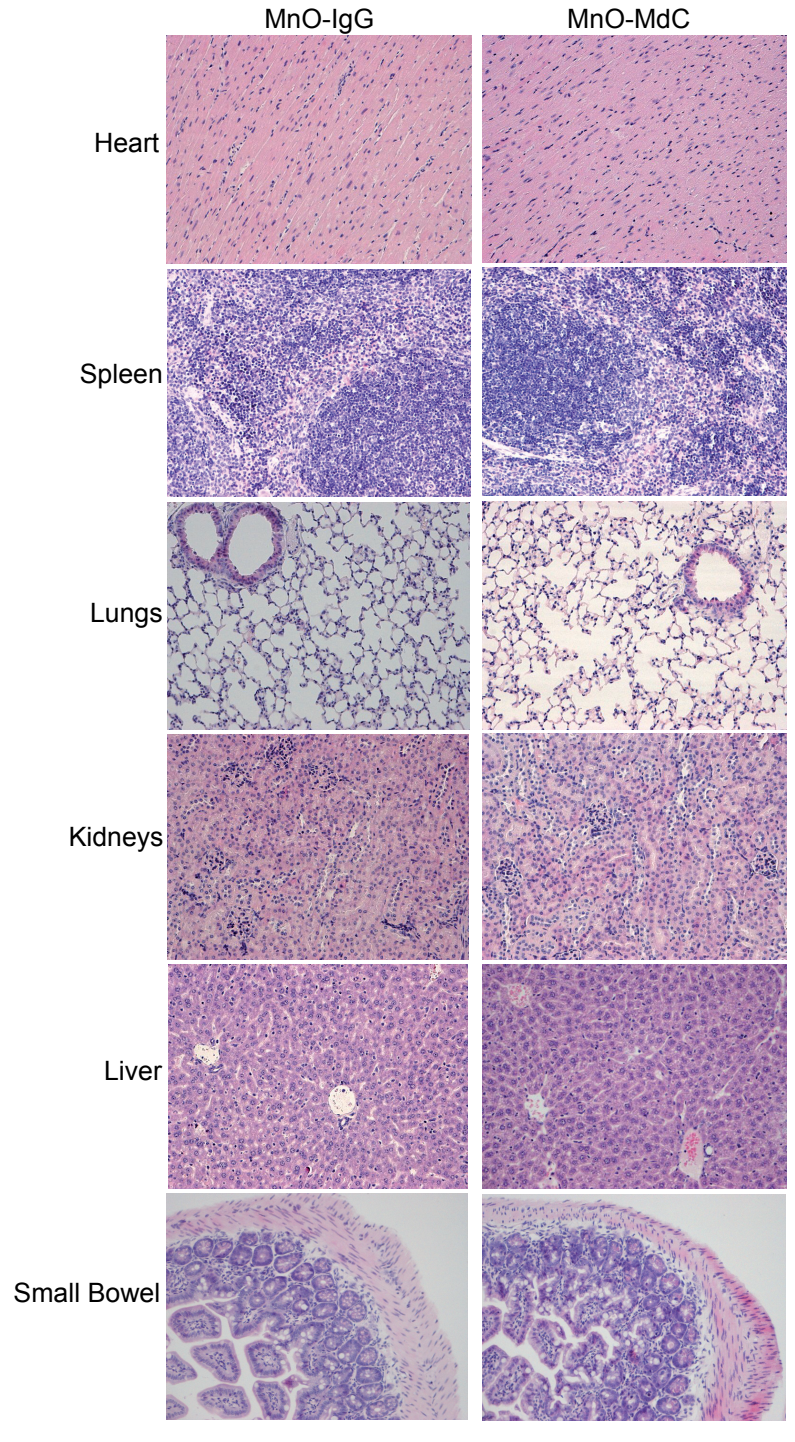
MnO-IgG
MnO-MdC
Heart
Spleen
Lungs
Kidneys
Liver
Small Bowel